Chem. Res. Chinese Universities, 2019, 35(6), 957—961 doi: 10.1007/s40242-019-9172-8

Preparation and Pseudo-capacitance Performance of $NiCo_2O_4$ Nanosheets

ZHOU Qi[1,2*], JIAO Sunzhi[1], ZHENG Bin[1] and LI Zhiyang[1]

1. School of Materials Science and Engineering, Lanzhou University of Technology, Lanzhou 730050, P. R. China;
2. State Key Laboratory of Advanced Processing and Recycling of Non-ferrous Metals, Lanzhou University of Technology, Lanzhou 730050, P. R. China

Abstract Ternary nickel cobaltite($NiCo_2O_4$), as a promising electrode material for supercapacitors, has attracted increasing attention for its excellent electrochemical properties. In this study, novel $NiCo_2O_4$ nanosheets were rationally designed and prepared using dealloying process, followed by an oxidation treatment. The as-prepared sample was characterized by microstructural and electrochemical techniques in view of its possible application in supercapacitors. The as-prepared sample exhibited high specific capacitance and excellent durability. The specific capacitance reached 663 F/g at 1 A/g and the rate capacitance high up to 73.6% when the current density increased from 1 A/g to 20 A/g. After 5000 cycles of galvanostatic charge-discharge durability test at 4 A/g, the capacity retention rate was 82.1%. The results indicate that versatile dealloying can be used to prepare robust electrode for supercapacitor application.

Keywords Rapid-solidification; Dealloying; Nickel cobaltate; Nanosheet; Pseudo-capacitance

1 Introduction

Supercapacitors(SCs), as promising energy-storage devices, have attracted increasing attention owing to their high power density, fast charge/discharge process, long lifespan, and adequate security[1—5]. However, the mass production and application of SCs are seriously hindered for the lack of well-performed and reasonably priced electrode materials. Up to now, the developed materials for SCs can be classified into carbonaceous materials, conducting polymers, and transition metal oxides(TMOs). Although the former shows very large specific surface area, good conductivity, and excellent durability, the specific capacitance is relatively low when compared with TMOs. For polymers, the corresponding stability is not satisfactory. In contrast, researchers have focused on TMOs, such as RuO_2[6—9], NiO[10—12], Co_3O_4[13—16], MnO_x[17—19], and $NiCo_2O_4$[20—22]. RuO_2 may be the state-of-the-art material due to its ultrahigh specific capacitance and excellent durability, while the extravagant price and poor environment effect limit its extensive commercial applications[23]. For other single-metal oxides, the semiconducting property blocks its performance to be fully exerted. In recent years, binary metal oxides have been proved to be promising for SCs, of which the spinel $NiCo_2O_4$ possesses intriguing advantages of better electrical conductivity and higher redox activity than those of single-metal oxides, such as NiO and Co_3O_4[20]. So far, the common methods for preparing $NiCo_2O_4$ are sol-gel, electrospinning, electrodeposition, hydrothermal method, chemical coprecipitation, and template method[24]. Special topography, such as zero-dimensional (0D) nanodot structure, one-dimensional(1D) nanorod structure, or two-dimensional(2D) nanosheet structure can be obtained using the above methods. Also, the product exhibits satisfactory capacitance performance. The sol-gel method is suitable for the preparation of 0D nanoparticles, electrospinning is suitable for structuring 1D fibers with a diameter in the range of micro to nano scale, and electrodeposition holds a merit for structuring self-supporting electrode materials, where the electroactive material is grown directly on a conductive substrate. Hydrothermal method is suitable for reactions requiring mild reaction conditions, and high controllability is widely used to synthesize various nanomaterials, although chemical coprecipitation method is known by simplicity of operation steps, the final product purity is often unsatisfactory. The template method is promising for structuring interconnected 3D hierarchical, porous or continuous channels. The above-mentioned methods hold individual characteristics of advantages and disadvantages. A common disadvantage in using $NiCo_2O_4$ is the unsatisfactory durability during the cycling test, which cannot be matched with large capacity. Fu *et al*.[25] prepared $NiCo_2O_4$ nanosheets grown on foamed nickel *via* composite electrodeposition. Although the specific capacitance reached 2517 F/g, the capacitance retention rate was as low as 64% after 800 cycles at a current density of 8 A/g. Jokar *et al*.[26] prepared $NiCo_2O_4$ nanorods *via* hydrothermal reaction; $NiCo_2O_4$ exhibited a higher specific capacitance of 758 F/g at 1 A/g, while the specific capacitance loss rate after 1500 cycles galvanostatic charge-discharge(GCD) at 5 A/g was 20%. Zhang *et al*.[27] synthesized porous spinel $NiCo_2O_4$ by chemical co-precipitation method and obtained a large specific surface area of 82.6 m^2/g, while the specific capacity of 218 F/g at 0.1 A/g and capacity

*Corresponding author. Email: zhouxq@lut.edu.cn

Received June 21, 2019; accepted September 4, 2019.
Supported by the National Natural Science Foundation of China(No.51661018).

retention rate of 65% was unsatisfactory. It is well accepted that grain pulverization and agglomeration occur during accumulation of stress caused by the large volume change during the charge and discharge process, and this greatly damages the durability of the electrode material. Dealloying, namely, the metal template method, as a novel material design strategy, has been demonstrated as a versatile and convenient channel for preparing porous materials characterized high structural definition, short electron-/ion-transport pathways, and high specific surface area[28], the special porous structure constructed *in situ* by template removal are usually uniform in size and structurally robust. As a result, excellent mechanical stability and strong resistance to volume expansion are expected to improve the durability of the electrode material. Wang *et al*.[29] fabricated mesoporous $NiCo_2O_4$ by electrodeposition combined with dealloying method; $NiCo_2O_4$ exhibited a high specific surface area of 87.4 m^2/g and only 8.4% area specific capacity loss after 50000 cycles GCD test. As per our knowledge, there are few other reports about de-alloyed materials used as electrode in SCs. Hence, it is promising to combine spinel $NiCo_2O_4$ with the dealloying technique.

In this work, we reported the preparation of porous $NiCo_2O_4$ nanosheets. The construction process and extensive investigation about phase composition, morphology, microstructure and electrochemical performance were presented and described in detail, aiming to explore new possibility to prepare well-performed pseudo-capacitance electrode materials and expand the applications of dealloying.

2 Experimental

2.1 Preparation of Ni-Co Precursor and $NiCo_2O_4$

All the used chemical reagents were of analytical grade and used without further purification. All metal powders (99.9%, 200 mesh) were purchased from Chinese brand suppliers. The specific preparation process is as follows: pure commercial nickel, cobalt, and aluminum powders as the starting materials were mixed in an atomic ratio of 3.3:6.7:90 and then milled for 5 h. Afterwards, the mixture was pressed into column-like billet with an isostatic pressing machine (CIP-22M, Shenyang, China) and then melted in a high-frequency vacuum inductance furnace. The cast alloy was melted again and molded into a rotating copper roller(linear velocity: 18 m/s) under high-pressure argon. The Ni-Co-Al bands obtained under rapid solidification were free etched in an oxygen-free NaOH aqueous solution(25%, mass fraction) at 65 °C for 30 h to remove Al. The de-alloyed Ni-Co was rinsed with deionized water and ethanol several times. Finally, $NiCo_2O_4$ was obtained by annealing the Ni-Co at 350 °C for 2 h in a muffle furnace (SX-G18123, Tianjin, China).

2.2 Material Characterization

The morphological features and elemental mapping were measured using field-emission scanning electron microscopy (FE-SEM, JSM-6700F) combined with energy-dispersive X-ray spectroscopy(EDX) and transmission electron microscopy(TEM, JEM-2010). The crystalline phases were obtained using powder X-ray diffraction(XRD, D/Max-2400) with Cu $K\alpha$ radiation(λ=0.15418 nm). The surface chemical elements and chemical bonding states of the elements were evaluated using X-ray photoelectron spectroscopy(XPS, ESCALab 250 XI). The surface area and porosity were evaluated on a Brunauere-Emmette-Teller micromeritics surface area analyzer (BET, ASAP 2020).

2.3 Electrode Preparation and Electrochemical Characterization

The electrode was formulated with accurately weighed active materials, acetylene black, conductive graphite, and polytetrafluoroethylene emulsion(80:7.5:7.5:5). The resultant slurry was pressed over preprocessed nickel foam and dried at 60 ℃ for 10 h in a vacuum oven. A typical three-electrode glass cell equipped with a composite electrode, platinum plate, and saturated calomel electrode was used for electrochemical measurements in 2 mol/L KOH aqueous solution. Electrochemical characterization techniques, including cyclic voltammetry(CV), GCD, electrochemical impedance spectroscopy(EIS), and durability test, were used in the support of CHI660E electrochemical workstation.

3 Results and Discussion

3.1 Material Characterization

The XRD pattern[Fig.1(A)] indicates that the as-prepared Ni-Co alloy was dominated by nickel-cobalt solid solution combined with small amount phases of $Ni(OH)_2{\cdot}0.75H_2O$ and $Co(OH)_2$. No diffraction information of the aluminum phase was detected. The XRD pattern in Fig.1(B) corresponds well

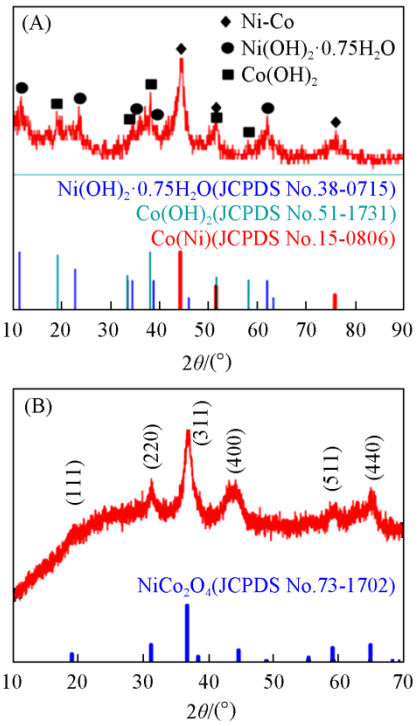

Fig.1 XRD patterns of Ni-Co(A) and $NiCo_2O_4$(B)

with the standard diffraction peaks of cubic spinel $NiCo_2O_4$ [JCPDS No.73-1702, space group *Fd3m*(227)][22].

The survey spectra of XPS results[Fig.2(A)] contain Ni_{2p}, Co_{2p}, and O_{1s} and indicate the existence of Ni, Co, and O without any other impurities. The C_{1s} peak at 283.0 eV is related to some surface adventitious carbon-based contamination. High-resolution spectrum of Ni_{2p} is well fitted with two spin-orbit doublets corresponding to Ni^{2+} and Ni^{3+} by Gaussian fitting. Specifically, the peaks at 854.8 and 872.16 eV are assigned to Ni^{2+} and peaks at 856.2 and 873.5eV are related to Ni^{3+}[21]. In a similar way, the peaks[Fig.2(C)] at 779.76 and 794.9 eV correspond to Co^{2+}, while peaks at 781.03 and 796.24 eV belong to Co^{3+}[30]. For O_{1s}[Fig.2(D)], the peak at 529.8 eV is assigned to the metal-oxygen bond, and the peak at 531.22 eV is associated to oxygen in the hydroxyl group[21]. Moreover, no Al_{2p} signal is detected[Fig.2(E)], implying complete removal of Al from the surface of $NiCo_2O_4$. This result is consistent with the aforementioned XRD information.

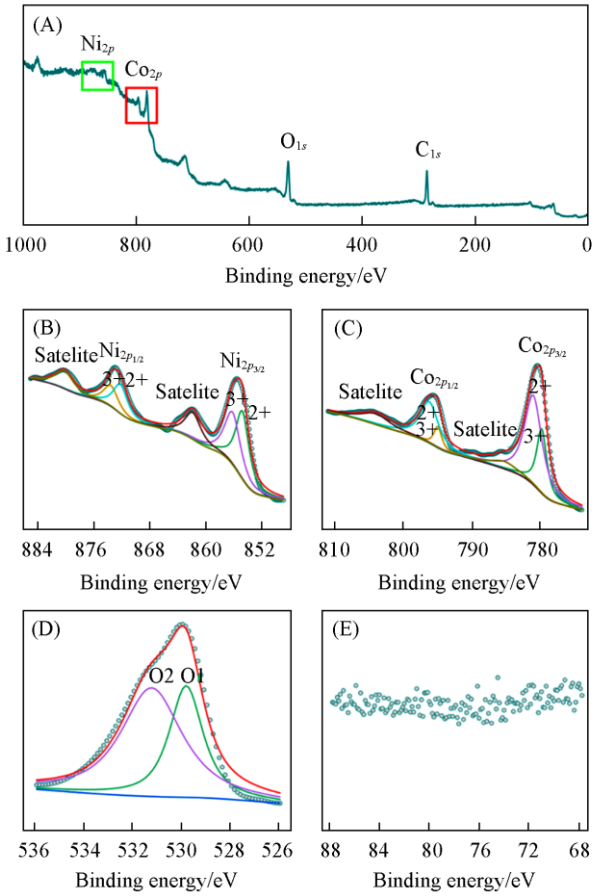

Fig.2 XPS spectra of $NiCo_2O_4$

(A) Survey scan; (B) Ni_{2p}; (C) Co_{2p}; (D) O_{1s}; (E) Al_{2p}.

The morphology and microstructure information of the Ni-Co precursor and the as-prepared $NiCo_2O_4$ were examined using FE-SEM and TEM(Fig.3). It can be clearly seen that the Ni-Co precursor[Fig.3(A)] is characterized with 2D nanosheets with a diameter of 200—500 nm and a thickness of 15—20 nm. The uniquely distributed 2D nanosheets were resulted from the dissolution of Al and self-assembly of Co and Ni during the etching processing. With the dissolution of Al at the surface layer of Ni-Co-Al, numerous Ni and Co atoms were exposed to the solid-liquid interface and then diffused and aggregated into clusters, finally growing into nanosheets. Compared with Ni-Co alloy obtained from $Ni_{1.7}Co_{3.3}Al_{95}$[31], the reduction in aluminum content($Ni_{3.3}Co_{6.7}Al_{90}$) makes the arrangement of interconnected Ni-Co nanosheet more random and structurally robust. The as-prepared $NiCo_2O_4$ inherited the original nanosheet structure[Fig.3(B) and (C)] and showed a rougher surface, which is similar with that of our previous reported $NiCo_2O_4$ and $NiMoO_4$[31,32]. The calcining process led to water loss when hydroxide transformed into oxides, resulting in the wrinkle and roughening of nanosheets, which further increased the specific surface area. The elemental mapping images of the as-prepared $NiCo_2O_4$[Fig.3(D)] indicate that the Ni, Co, and O elements are uniformly dispersed in the nanosheet structure. The TEM image of $NiCo_2O_4$[Fig.3(E)] revealed that there are finer mesoporous structures in the skeletons, which further increase specific surface area and provide more active sites, resulting in a satisfactory electrochemical performance. The clear lattice fringes in the HRTEM image[Fig.3(F)] show one interplanar distance of 0.458 nm, which is perfectly in agreement with the (111) crystal face of $NiCo_2O_4$. The inspection of the diffraction rings in the corresponding selected-area electron diffraction(SAED) pattern[inset of Fig.3(F)] indicates that the final product was a polycrystalline material. Similarly, the result is consistent with XRD analysis.

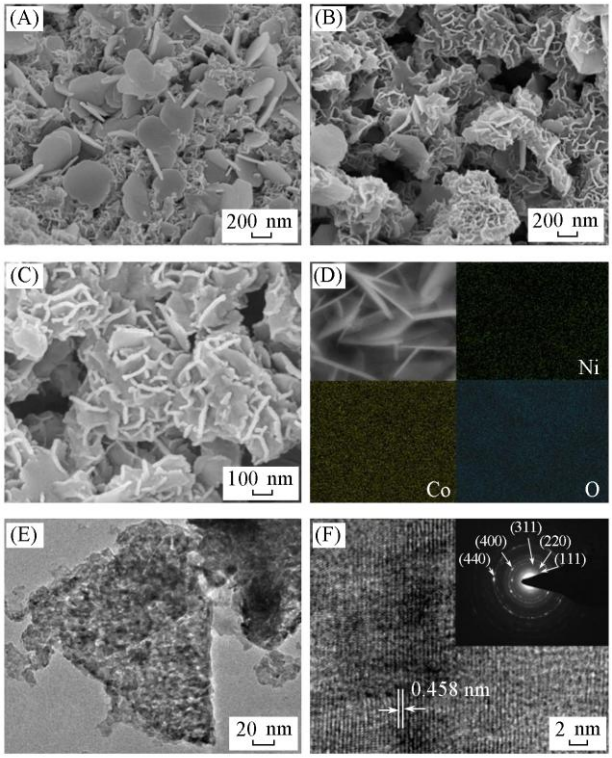

Fig.3 SEM images of Ni-Co(A) and $NiCo_2O_4$(B, C), elemental mapping(D), TEM(E) and HRTEM images of $NiCo_2O_4$(F)

Inset of (F) is the corresponding SAED pattern.

Generally speaking, the electrochemical performance of an electrode is closely related to its specific surface area. Therefore, BET surface area test was further performed on the as-prepared $NiCo_2O_4$ nanosheets using nitrogen adsorption and

desorption, which was measured at 77 K to give a quantitative specific surface area values and mesopore information observed in the aforementioned TEM. As the results shown in Fig.4, a BET surface area of 53.68 m^2/g, an average pore diameter of 14.26 nm, and a mesoporous structure with a pore size of less than 10 nm were obtained using the Barrette-Joynere-Halenda(BJH) method. These mesoporous structures cooperated with the electrolyte buffer formed by interconnected nanosheets are beneficial for fast ion transfer at the electrode/electrolyte interface, which may facilitate subsequent electrochemical measurement.

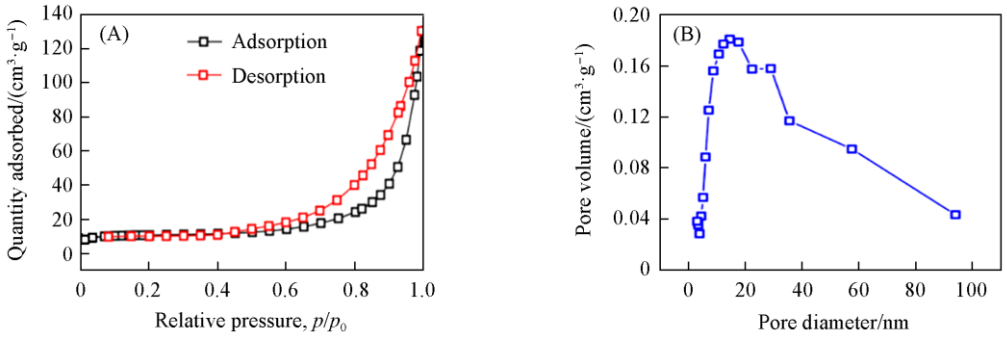

Fig.4 N_2 adsorption-desorption isotherm(A) and pore size distribution plot(B) of $NiCo_2O_4$ nanosheets

3.2 Electrochemical Characterization

The obvious redox peak formed by charge transfer between M^{2+}/M^{3+}(M=Ni, Co) and Co^{3+}/Co^{4+} can be seen from CV curves[Fig.5(A)], where the fast and reversible Faradaic reactions occur[22]. Theoretically, there should be two pairs of peaks. However, the close proximity of the redox potentials of Ni^{2+}/Ni^{3+} and Co^{3+}/Co^{4+} led to the emergence of only a significant pair of peaks[33]. The similar shape under various scan rate indicates lower degree of polarization.

The shape of the GCD curves[Fig.5(B)] exhibited a quasi-triangular symmetrical distribution with a curvature. This is the

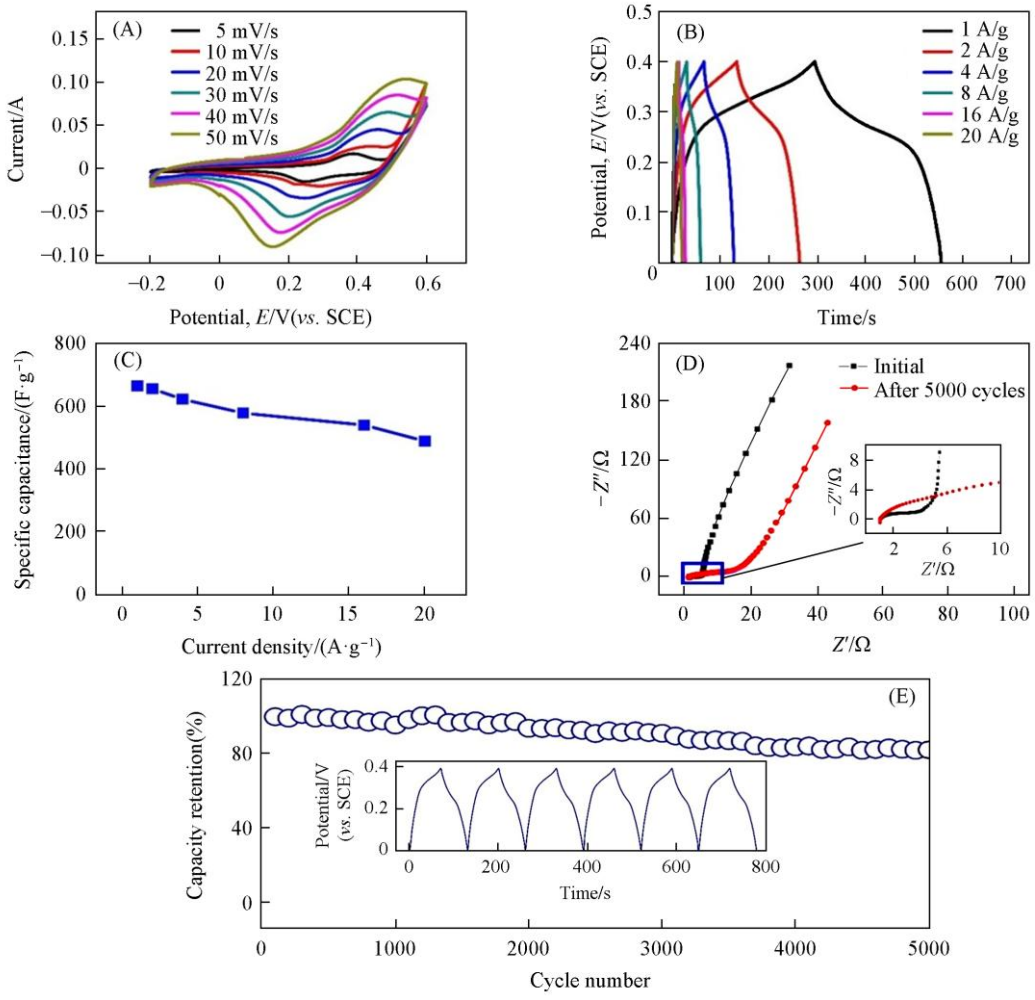

Fig.5 CV curves(A), GCD curves(B), specific capacitance to current curve(C), Nyquist plots(D) and cycle life plot(E) of $NiCo_2O_4$

typical pseudocapacitive behavior of TMOs[17]. Obviously, the specific capacitance decreased with an increase in the current density[Fig.5(C)]. It was mainly resulted from the diffusion of electrolyte, and electron conduction involved in the Faraday reaction is limited under larger current density. In addition, the good symmetry of GCD curves indicates good process reversibility and coulombic efficiency. The specific capacitance retention at 20 A/g was 73.6% with respect to 1 A/g. EIS is also one of the important tools to help understand the reactivity of the SC. Hence, the as-prepared $NiCo_2O_4$ is subjected to EIS studies in the frequency range of 100 kHz to 0.01 Hz. The Nyquist plots[Fig.5(D)] showed minor semicircular in high frequency region, which is directly related to the reduced R_{ct}[30]. Importantly, the minor change in R_{ct} and a specific capacity retention of 82.1%[Fig.5(E)] after prolonged 5000 cycles GCD at 4 A/g show excellent durability of the as-prepared $NiCo_2O_4$. Compared with the literature[27,34—36], dealloying-prepared $NiCo_2O_4$ nanosheets exhibited high specific capacity and satisfactory durability, which resulted from large specific surface area and good mechanical stability of the as-prepared active materials. Although the relatively low content of aluminum reduces the specific surface area and thus decreases the specific capacity, the cycling durability of $NiCo_2O_4$ was not reduced compared with that of our previously prepared $NiCo_2O_4$[31] with an aluminum abundance of 95%. All these results confirm that the dealloying construction of porous spinel $NiCo_2O_4$ is a promising method to prepare novel electrode materials that can have energy storage applications.

4 Conclusions

Selective corrosion can be used to obtain a porous nanosheet structure. The oxides formed *in situ* on the surface of a precursor exhibit a maximum capacitance of 663 F/g at 1 A/g and good cycle stability, with a capacity retention rate of 82.1% after 5000 cycles GCD at 4 A/g. The well electrochemical performance of $NiCo_2O_4$ nanosheets is mainly attributed to the following. (1) The spinel crystal structure enables $NiCo_2O_4$ to have more free electrons and holes to improve the conductivity. (2) Dealloying provides $NiCo_2O_4$ with a high specific surface area of 53.68 m^2/g, which accelerates the electrochemical kinetics by not only increasing the contact area of the active substance with the electrolyte to a large extent but also acting as a buffer for the electrolyte. (3) The special interconnected nanosheet structure imparts good mechanical stability to the electrode material. Furthermore, this materials processing method could be applied to prepare other porous materials for energy storage or catalysis applications.

References

[1] Simon P., Gogotsi Y., *Nature Materials*, **2008**, *7*(11), 845

[2] Zhang L. L., Zhao X. S., *Chem. Soc. Rev.*, **2009**, *38*(9), 2520

[3] Snook G. A., Kao P., Best A. S., *J. Power Sources*, **2011**, *196*(1), 1

[4] Zhao J., Jiang Y., Fan H., Liu M., Zhuo O., Wang X., Wu Q., Yang L., Ma Y., Hu Z., *Adv. Mater.*, **2017**, *29*(11), 1604569

[5] Zou Y., Cai C., Xiang C., Huang P., Chu H., She Z., Xu F., Sun L., Kraatz H. B., *Electrochim. Acta*, **2018**, *261*, 537

[6] Bi R. R., Wu X. L., Cao F. F., Jiang L. Y., Guo Y. G., Wan L. J., *The Journal of Physical Chemistry C*, **2010**, *114*(6), 2448

[7] Xia H., Meng Y. S., Yuan G., Cui C., Lu L., *Electrochemical and Solid-state Letters*, **2012**, *15*(4), A60

[8] Zhai S., Wang C., Karahan H. E., Wang Y., Chen X., Sui X., Huang Q., Liao X., Wang X., Chen Y. J. S., *Small*, **2018**, *14*(29), 1800582

[9] Arunachalam R., Prataap R. K. V., Raj R. P., Mohan S., Vijayakumar J., Peter L., Al Ahmad. M., *Surface Engineering*, **2019**, *35*(2), 103

[10] Liu M., Wang X., Zhu D., Li L., Duan H., Xu Z., Wang Z., Gan L., *Chem. Eng. J.*, **2017**, *308*, 240

[11] Ouyang Y., Xia X., Ye H., Wang L., Jiao X., Lei W., Hao Q., *ACS Applied Materials & Interfaces*, **2018**, *10*(4), 3549

[12] Jiao Y., Hong W., Li P., Wang L., Chen G., *Appl. Catal. B: Environ.*, **2019**, *244*, 732

[13] Pang H., Li X., Zhao Q., Xue H., Lai W. Y., Hu Z., Huang W., *Nano Energy*, **2017**, *35*, 138

[14] Qiu D., Ma X., Zhang J., Zhao B., Lin Z., *Chem. Phys. Lett.*, **2018**, *710*, 188

[15] Shi Z., Xing L., Liu Y., Gao Y., Liu J., *Carbon*, **2018**, *129*, 819

[16] Raj S., Srivastava S. K., Kar P., Roy P., *Electrochim. Acta*, **2019**, *302*, 327

[17] Chen S., Zhu J., Wu X., Han Q., Wang X., *ACS Nano*, **2010**, *4*(5), 2822

[18] Chi H. Z., Wu Y. Q., Shen Y. K., Zhang C., Xiong Q., Qin H., *Electrochim. Acta*, **2018**, *289*, 158

[19] Xie Y., Yang C., Chen P., Yuan D., Guo K., *J. Power Sources*, **2019**, *425*, 1

[20] Zhang G., Lou X. W., *Adv. Mater.*, **2013**, *25*(7), 976

[21] Wang T., Guo Y., Zhao B., Yu S., Yang H. P., Lu D., Fu X. Z., Sun R., Wong C. P., *J. Power Sources*, **2015**, *286*, 371

[22] Bhagwan J., Nagaraju G., Ramulu B., Sekhar S. C., Yu J. S., *Electrochim. Acta*, **2019**, *299*, 509

[23] Chen W. C., Hu C. C., Wang C. C., Min C. K., *J. Power Sources*, **2004**, *125*(2), 292

[24] Li Y., Han X., Y T. F., He Y. B., Li X. F., *J. Energy Chem.*, **2019**, *31*, 54

[25] Fu H. Y., Wang Z. Y., Li Y. H., Zhang Y. F., *Mater. Res. Innov.*, **2015**, *19*(Suppl. 4), S255

[26] Jokar E., Iraji Zad A., Shahrokhian S., *J. Solid State Electr.*, **2015**, *19*(1), 269

[27] Zhang Y., Wang S. W., Gao H. L., Zhao S. Q., *Chinese Journal of Power Sources*, **2018**, *42*(2), 212

[28] Weissmüller J., Sieradzki K., *Mrs. Bull.*, **2018**, *43*(1), 14

[29] Wang N., Sun B. L., Zhao P., Yao M., Hu W. C., Komarneni S., *Chem. Eng. J.*, **2018**, *345*, 31

[30] Feng X., Huang Y., Li C., Chen X., Zhou S., Gao X., Chen C., *Chem. Eng. J.*, **2019**, *368*, 51

[31] Zhou Q., Zheng B., Wang Y. F., Zheng S. Z., *J. Materials Science Engineering of Powder Metallurgy*, **2016**, *21*(5), 795

[32] Zhou Q., Zheng B., Li Z. Y., Wang Y. F., Feng J. W., *Chinese Journal of Inorganic Chemistry*, **2017**, *33*(8), 1416

[33] Pang M. J., Jiang S., Long G. H., Ji Y., Han W., Wang B., Liu X. L., Xi Y. L., Xu F. Z., Wei G. D., *RSC Advances*, **2016**, *6*(72), 67839

[34] Sun J., Wang W., Yu D., *J. Electron. Mater.*, **2019**, *48*(6), 3833

[35] Li W., Yang F., Hu Z., Liu Y., *J. Alloy. Compd.*, **2018**, *749*, 305

[36] Fu H. Y., Wang Z. Y., Li Y. H., Zhang Y. F., *Mater. Res. Innov.*, **2015**, *19*, S255